JOURNAL OF SOLID STATE CHEMISTRY **121,** 362–371 (1996)
ARTICLE NO. 0049

$Hf_{5.08}Mo_{0.92}P_3$, a New Mixed Transition-Metal Phosphide: Structure, Bonding, and Site Preferences

Jun Cheng and Hugo F. Franzen[1]

Department of Chemistry and Ames Laboratory-DOE, Iowa State University, Ames, Iowa 50011

Received June 5, 1995; accepted October 12, 1995

A new structure type which is similar to that of many known binary early transition-metal phosphides, sulfides, and selenides has been found in the ternary Hf–Mo–P system. The compound $Hf_{5.08}Mo_{0.92}P_3$ has been synthesized by high-temperature techniques and characterized by single-crystal X-ray diffraction. The space group is *Pnma* (no. 62) with lattice parameters a = 18.231(7), b = 3.537(1), c = 9.695(5), Z = 4. The strength of the metal–metal and metal–phosphorus bonding in different metal sites in Hf_2P and $Hf_{5.08}Mo_{0.92}P_3$ has been determined by both Pauling bond orders (PBO) and Mulliken overlap populations (MOP) from extended Hückel tight-band calculations. Site preferences of the two metals in $Hf_{5.08}Mo_{0.92}P_3$ are evaluated by MOP analysis

INTRODUCTION

Early transition-metal-rich sulfides, selenides, and phosphides (1) show a variety of interesting structures and bonding arrangements. Both metal–metal bonding and metal–nonmetal bonding make important contributions to the structures. One type of structure found for these compounds shares the following characteristics: (a) a short axis which is perpendicular to mirror planes which contain all elements; (b) the nonmetal is capped trigonal-prismatic coordinated; (c) the metal coordination is related to or reminiscent of bcc. Compounds such as Ti_2S (2), Ti_8S_3 (3), Nb_7P_4 (4), $Zr_{14}P_9$ (5), $Nb_{21}S_8$ (6), and $Nb_{14}S_5$ (7) belong to this group. Recently, two ternary Nb–Ta sulfides (8, 9) and one ternary Zr–Nb phosphide (10) were found to form in structures of this general type with fractional occupancy of metal sites by long-range averaging of Nb and Ta or Zr and Nb, respectively. Since these ternary structures are unknown among the binaries, it is believed that long-range averages of transition metals can have different structural chemistry than do the corresponding binaries (11). The compounds form from the respective binaries as a result of a combination of entropic stabilization and electronic effects.

No metal-rich molybdenum chalcogenide (with M/Ch ratio >1) is known, probably because of the instability of these "compounds" with respect to the disproportionation reaction to form Mo metal and other known non-Mo-rich compounds. As for phosphides, Mo-rich compounds such as Mo_5P_3 (12), Mo_8P_5 (13), and Mo_3P (14) are known. This fact demonstrates that Mo-rich phosphides are at least stable with respect to disproportionation. The ternary E–Mo–P (E = early transition metals) system could yield, consistent with the stabilization ideas mentioned above, new structures and chemistry because of the stronger (relative to E) metal bonding character brought to it by Mo. In an effort to test this idea, we investigated the Hf–Mo–P system and some new compounds (15) were synthesized. Here we report a new ternary phosphide, $Hf_{5.08}Mo_{0.92}P_3$, its synthesis, and its structure as determined by single-crystal X-ray diffraction. The metal–metal bonding and metal–phosphorous bonding characteristics of different metal sites of both $Hf_{5.08}Mo_{0.92}P_3$ and Hf_2P are evaluated via the scales of Pauling bond orders (PBO) and Mulliken overlap populations (MOP) from extended Hückel calculation. Site preferences of different metals in $Hf_{5.08}Mo_{0.92}P_3$ are also analyzed by Mulliken overlap populations.

SYNTHESIS

A sample with the initial stoichiometry Hf_2MoP was prepared from the appropriate quantities of Hf, Mo, and previously synthesized HfP, pelletized, and arc-melted twice for 30 seconds each time (10 V, 60 A) with inversion of the sample between each arc melting. The arc-melted sample was annealed at about 1700°C by induction heating. This temperature is just below the temperature at which the sample begins to melt. The annealing time is about 4–5 hours and the residual pressure is below 10^{-7} Torr. Large needle-shaped crystals were picked from a broken chunk and later were examined by single-crystal X-ray diffraction.

X-RAY SINGLE-CRYSTAL EXPERIMENT AND REFINEMENT

Intensity data sets were collected for the crystal on the rotating anode Rigaku AFC6R four-circle diffractometer

[1] To whom correspondence should be addressed.

0022-4596/96 $18.00

TABLE 1
Crystal Data for $Hf_{5.08}Mo_{0.92}P_3$

Formula	$Hf_{5.08}Mo_{0.92}P_3$
Space group	*Pnma* (no. 62)
a (Å)	18.231(7)
b (Å)	3.537(1)
c (Å)	9.695(5)
v (Å^3)	625.1(1)
z	4
d_{calc} (g/cm^3)	11.487
μ (Mo$K\alpha$)	845.05 cm^{-1}
Data collection instrument	Rigaku AFC6R
Radiation (monochromated in incident beam)	Mo ($K\alpha$ = 0.71069)
Scan method	$\omega - 2\theta$
Octants measured	$h \pm k \pm l$
Data collection range, 2θ (degrees)	0–60.1
No. refl. measured	3916
No. unique data, total	1888
With $F_0^2 > 3\sigma(F_0^2)$	598
No. parameters refined	49
Absorption correction	Ches
Trans. factors, max., min.	0.46–1.03
Secondary ext. coeff. (10^{-7})	0.59624
R^a; R_w^b; GOF^c	0.050; 0.050; 1.64

[a] $R = \Sigma||F_0| - |F_c||/\Sigma|F_0|$.
[b] $R_w = [\Sigma w(|F_0| - |F_c|)^2/\Sigma w|F_0|^2]^{1/2}$; $w = 1/\sigma^2(|F_0|)$.
[c] GOF $= \Sigma((|F_0| - |F_c|)/\sigma_i)/(N_{obs} - N_{parameter})$.

(50 kV, 140 mA) using monochromatic MoKα X-ray radiation (λ = 0.71069 Å) and the ω-2θ scan technique out to 60° in 2θ. The observed intensities were corrected for Lorentz polarization, and an empirical absorption correction, using the program CHES (16), was applied, which resulted in transmission factors ranging from 0.46 to 1.03. The final least-square lattice parameters were calculated from Guinier X-ray powder camera FR552 using CuKα1 radiation and a NBS silicon internal standard. The crystal data for this new structure are summarized in Table 1.

The structure was solved by direct methods in space group *Pnma* (no. 62) and refined with anisotropic thermal parameters of the metal positions and with isotropic thermal parameters of the phosphorous positions to the final values R = 0.050 and R_w = 0.050 using TEXSAN (17) software. Initially, M1–M4 positions were taken to be occupied by Hf and the M5–M6 positions were taken to be occupied by Mo according to the peak heights in the electron density map. The thermal parameters for M5 and M6 gave quite large negative values, indicating that more electrons are needed in these positions. Mixing the occupancy of Mo and Hf at these two positions gave all positive thermal parameters. In a later anisotropic refinement the thermal parameter was well behaved. The mixing of Hf with Mo at the M1–M4 positions was also considered and gave negative occupancy of Mo at these sites, indicating no Mo on these sites. The final refined positions, occupancies,

TABLE 2
Positional Parameters and Occupancies for $Hf_{5.08}Mo_{0.92}P_3$

Atom	x	y	z	B_{eq}	%Hf	%Mo
M1	0.1619(2)	1/4	0.0257(3)	0.4(1)	100	
M2	0.3551(2)	1/4	0.0795(3)	0.4(1)	100	
M3	0.9700(2)	1/4	0.1224(3)	0.6(1)	100	
M4	0.7658(2)	1/4	0.7451(4)	0.6(1)	100	
M5	0.5067(3)	1/4	0.8888(4)	0.9(2)	62(3)	38
M6	0.1077(2)	1/4	0.3343(4)	0.5(2)	46(4)	54
P1	0.735(1)	1/4	0.034(2)	0.5(2)		
P2	0.120(1)	1/4	0.774(2)	0.7(3)		
P3	0.921(1)	1/4	0.848(2)	0.3(2)		

TABLE 3
***U* Values for $Hf_{5.08}Mo_{0.92}P_3$**

Atom	$u11$	$u22$	$u33$	$u13$
Hf1	0.003(2)	0.007(1)	0.007(1)	−0.003(1)
Hf2	0.008(2)	0.005(1)	0.003(1)	−0.001(1)
Hf3	0.007(2)	0.006(1)	0.009(1)	0.001(1)
Hf4	0.008(2)	0.007(1)	0.007(1)	0.000(1)
Hf5	0.010(3)	0.012(2)	0.012(2)	−0.001(2)
Hf6	0.006(3)	0.007(2)	0.005(2)	0.002(2)

TABLE 4
Interatomic Distances <4.0 Å in $Hf_{5.08}Mo_{0.92}P_3$

M1	M1–P2	2.56(2)	X1	M4	M4–P1	2.86(2)	X1
	M1–P3	2.63(1)	X2		M4–P3	3.01(2)	X1
	M1–P1	2.65(1)	X2		M4–M6	3.007(5)	X2
	M1–M4	3.131(4)	x2		M4–M4	3.5370(3)	X2
	M1–M6	3.151(5)	X1		M4–M2	3.298(4)	X2
	M1–M4	3.237(5)	X1		M4–M1	3.131(4)	X2
	M1–M3	3.312(4)	X2		M4–M2	3.543(5)	X1
	M1–M1	3.5370(3)	X2		M4–M1	3.237(5)	X1
	M1–M2	3.561(5)	X1	M5	M5–P2	2.59(2)	X1
	M1–M3	3.623(5)	X1		M5–P3	2.77(2)	X1
M2	M2–P2	2.62(1)	X2		M5–M6	2.784(5)	X2
	M2–P1	2.65(2)	X2		M5–M5	2.800(6)	X2
	M2–M6	3.039(4)	X2		M5–M5	3.5370(3)	X2
	M2–M5	3.094(5)	X2		M5–M3	3.159(4)	X2
	M2–M4	3.298(4)	X2		M5–M2	3.094(5)	X2
	M2–M5	3.325(5)	X1		M5–M6	3.255(7)	X1
	M2–M2	3.5370(3)	X2		M5–M2	3.325(5)	X1
	M2–M1	3.561(5)	X1	M6	M6–P3	2.56(1)	X2
	M2–M4	3.543(5)	X1		M6–P1	2.64(2)	X1
	M2–M3	3.570(5)	X1		M6–M5	2.784(2)	X2
M3	M3–P2	2.61(2)	X2		M6–M6	3.5370(3)	X2
	M3–P3	2.67(1)	X2		M6–M4	3.007(5)	X2
	M3–P3	2.80(1)	X1		M6–M2	3.039(4)	X2
	M3–M3	3.156(5)	X2		M6–M5	3.255(4)	X1
	M3–M5	3.159(4)	X2		M6–M3	3.245(5)	X1
	M3–M6	3.245(5)	X1		M6–M1	3.151(5)	X1
	M3–M3	3.5370(3)	X2	P	P1–P2	3.70(2)	X2
	M3–M1	3.312(4)	X2		P1–P1	3.5370(3)	X2
	M3–M1	3.623(5)	X1		P1–P2	3.65(3)	X1
	M3–M2	3.570(5)	X1		P2–P2	3.5370(3)	X2
M4	M4–P2	2.67(2)	X1		P2–P3	3.68(3)	X1
	M4–P1	2.71(1)	X2		P3–P3	3.5370(3)	X2

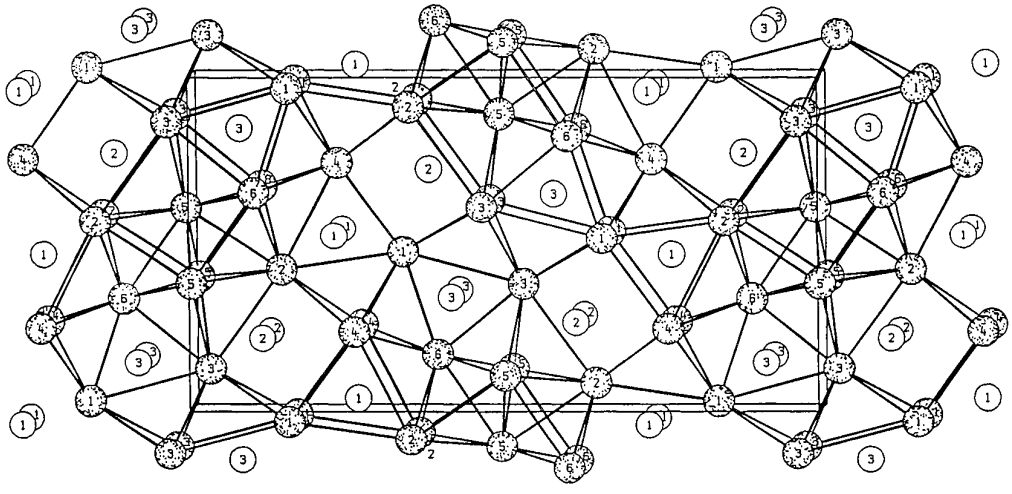

FIG. 1. $Hf_{5.08}Mo_{0.92}P_3$ structure viewing from [010] direction (M, shaded circles; P, open circles).

isotropic thermal parameters, and anisotropic thermal parameters are given in Tables 2 and 3, respectively. The interatomic distances (<4.0 Å) for this compound are given in Table 4.

STRUCTURE DESCRIPTIONS AND DISCUSSION

As mentioned in the introduction, this new ternary phosphide structure has general characteristics in common with many known structures of binary metal-rich sulfides, selenides, and phosphides. Examination of this new structure as depicted in Fig. 1 reveals known coordinations for all *M* and P.

All three phosphorous coordinations are slightly distorted capped trigonal prisms. For P1, the prism is vertical with two metal atoms capping the rectangular faces. For P2, the prism is horizontal with only one metal atom capping the rectangular face, and for P3, the prism is vertical but this time with all three rectangular faces capped by metals. The coordination environments of the three phosphorous are shown in Fig. 2. As for the metal environments (Fig. 3), M1 centers a fairly distorted bcc unit of metal atoms with two nonadjacent edges substituted by four phosphorous. An additional phosphorus caps one ''face'' with a short M1–P distance of 2.56 Å. M4 and M6 center a distorted bcc unit of metal with one edge substituted by two phosphorous. However M4 has three additional phosphorous neighbors while M6 only has one, which gives M6 a more metallic bonding environment. M5 centers a bcc unit of all metals with only two phosphorous capping the rectangular faces. M2 and M3 center pentagonal prisms of six metal atoms and two nonadjacent edges formed by four phosphorous atoms. Furthermore M3 has an additional phosphorous capping the face of a rectangular metal face. In addition, the M–P distances at M5 and M6 are similar to the other sites, while the M–M distances are significantly shorter (2.784(×2) Å, 2.800(×2) Å, four others around 3.1 Å for M5 and 2.784(×2) Å, 3.007(×2) Å, 3.039(×2) Å for M6) than those of other sites (usually the shortest bond distances are between 3.0 and 3.1 Å). Also at the M1–M4 sites, there are at least four phosphorus atoms are close to each metal, while there are only two and three phosphorus at M5 and M6 sites, respectively. This analysis of individual metal environments shows that M5 and M6 are the two metal sites with the strongest metal–metal bonding.

One can also describe this structure through packing of one large cluster unit shown in Fig. 4. This large cluster

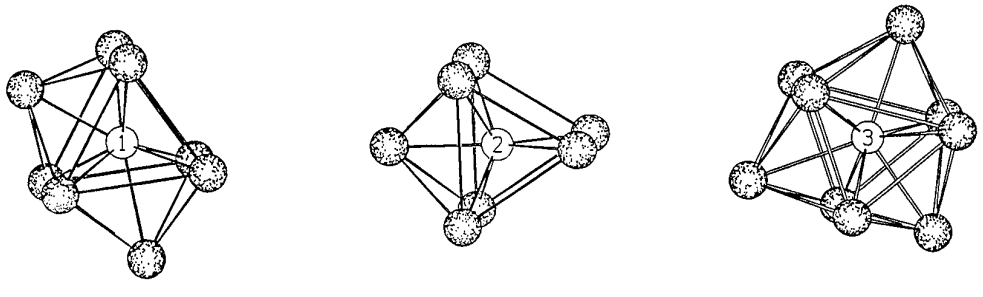

FIG. 2. Three kinds of phosphorus coordinations in $Hf_{5.08}Mo_{0.92}P_3$: P1 (left) P2 (middle), and P3 (right).

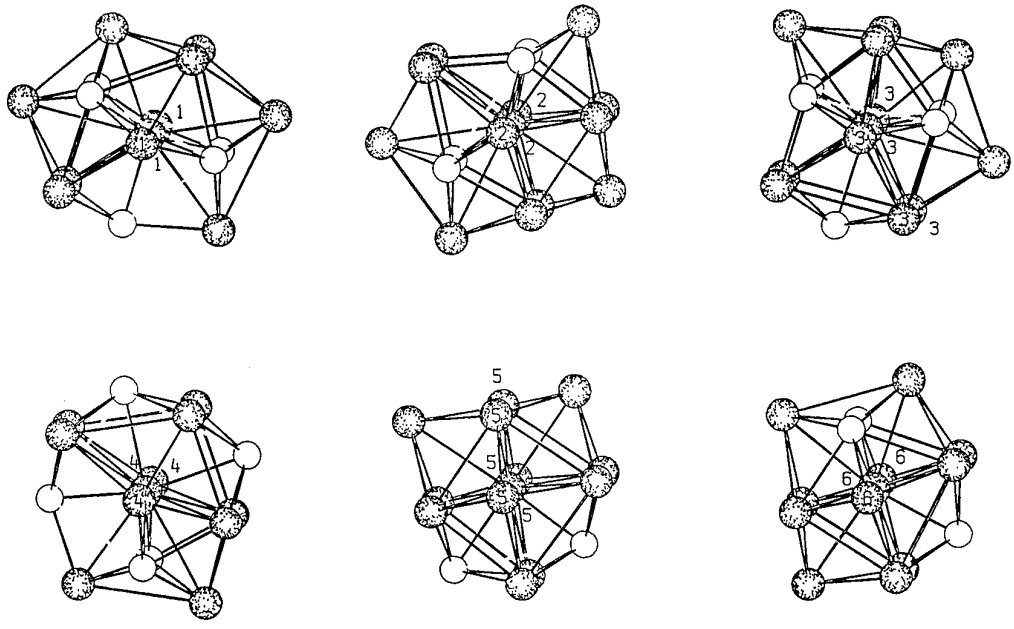

FIG. 3. Six kinds of metal environments in $Hf_{5.08}Mo_{0.92}P_3$: M1 to M3 (top from right to left); M4 to M6 (bottom from right to left).

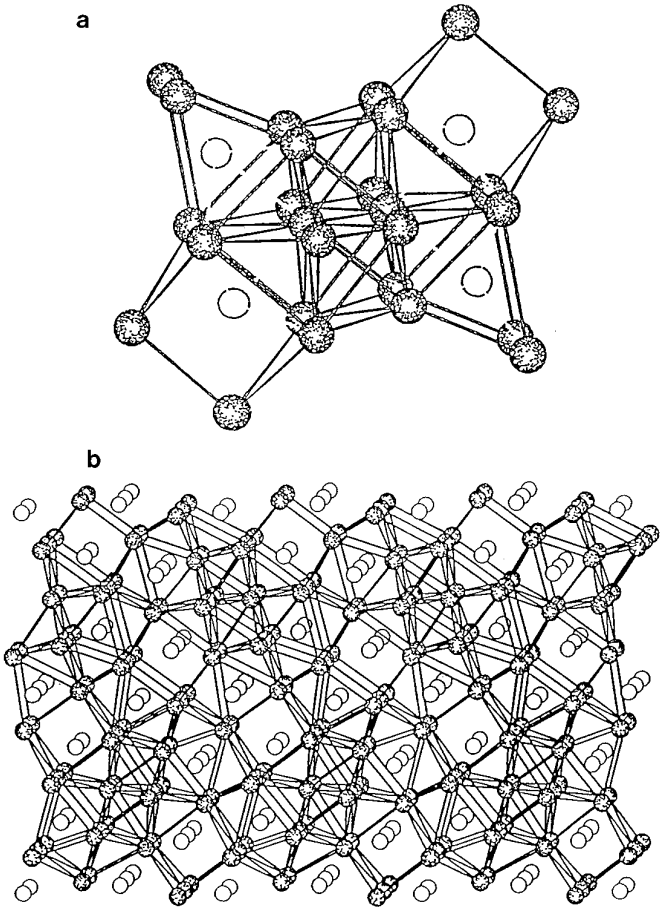

unit can be viewed as built by two ''fused'' cubes centered by M5 with the corner M5 of one cube being the center of the other and vice versa. The ''fused'' cubes have four faces available, and share these faces with four trigonal prisms. Two of these prisms are vertical and two are horizontal and they are *trans* oriented. Along the *c* direction, the ''fused'' cubes are connected by sharing two outside edges M1–M1 from the two prisms; in one cluster unit the edge is vertical and the other it is horizontal, and a corner atom M1, which is one of the outside corner atoms of a horizontal prism, is also the outside atom, of a vertical prism from another cube. Along the [220] and −[220] directions, the ''fused'' cubes pack without sharing atoms while two outside edges, M1–M1 and M4–M4, of the horizontal prism from one unit and one inner edge, M2–M2, of the horizntal prism from the other unit form a vertical trigonal prism where P1 is located.

Obviously with increasing metal/nonmetal ratio, the metal–metal interaction becomes more significant, which can structurally be easily seen in binaries by comparing the Ti_2S and Ti_8S_3 structures (Figs. 5a and 5b) or those of Nb_5Se_4 (18) and Nb_2Se (19) (Figs. 6a and 6b). Comparing

FIG. 4. (a) Two interpenetrated cubes with four faces shared by four trigonal prisms. Two of these trigonal prisms are vertical and two are horizontal and they are *trans* oriented. (b) The 3-D connection of the top units.

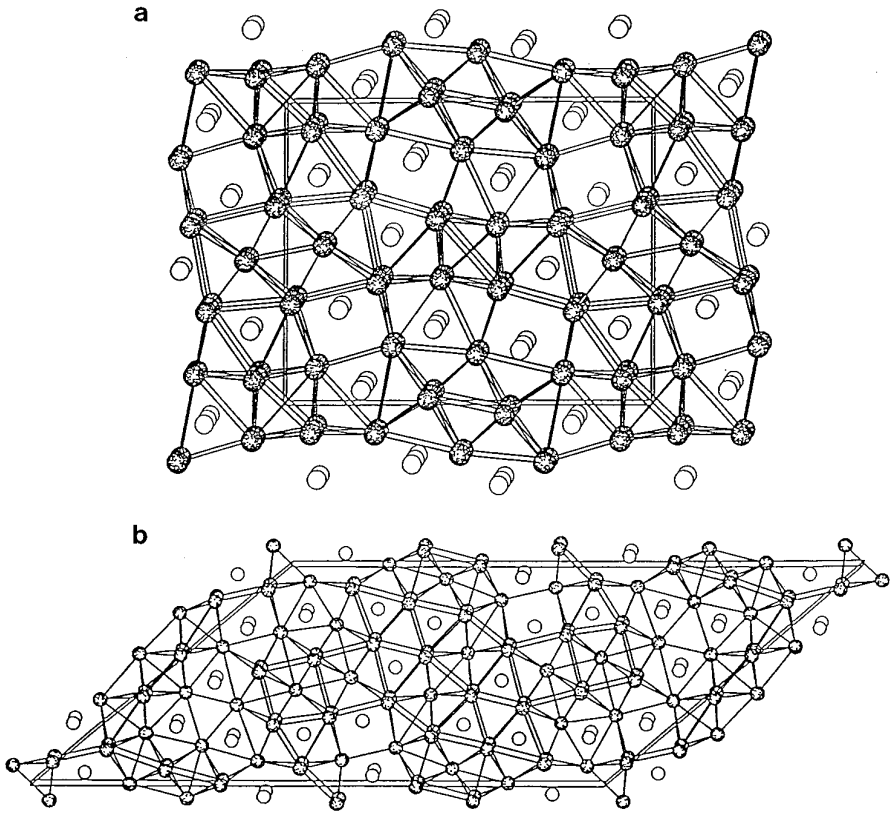

FIG. 5. The structure of Ti_2S (top, same structure type as Hf_2P) and Ti_8S_3 (bottom) viewed from the short axes.

Ti_2S to Ti_8S_3, one can see the metal "domain" in Ti_8S_3, while there are only face-sharing cubes in the Ti_2S structure. As for Nb_5Se_4 and Nb_2Se, isolated cubes in Nb_5Se_4 and "fused" cubes in Nb_2Se clearly show the increased significance of metal–metal bonding in Nb_2Se. If we compare the structure of Hf_2P (Ti_2S-type structure) with this new structure, the face-sharing cubes in Hf_2P and the "fused" cubes in this new structure can be seen. This suggests that the increased metal–metal bonding by Mo helps to stabilize the new building unit which leads to this new structure. The increased metal–metal bonding characteristic of this new structure is more obvious when we compare each metal environments in $Hf_{5.08}Mo_{0.92}P_3$ with those in Hf_2P (Fig. 7). The Hf1, Hf3, and M6 sites in $Hf_{5.08}Mo_{0.92}P_3$ are the same as the Hf2, Hf4, and Hf6 sites in Hf_2P. The Hf2 site in $Hf_{5.08}Mo_{0.92}P_3$ has a pentagonal prism environment similar to the Hf5 site in Hf_2P, except that there is an additional metal capping on the M_4-face in $Hf_{5.08}Mo_{0.92}P_3$, but not in Hf_2P. The M5 site in $Hf_{5.08}Mo_{0.92}P_3$ has an environment similar to the Hf3 site in Hf_2P except that in $Hf_{5.08}Mo_{0.92}P_3$ a metal replaces phosphorus to cap the "cube" face, and M5 is only coordinated by two phosphorus, whereas in Hf_2P Hf3 has three phosphorus neighbors. Hf4 in $Hf_{5.08}Mo_{0.92}P_3$ is similar to Hf1 in Hf_2P except that in Hf_2P, a metal replaces the pyramidal phosphorus which caps the M_4-face of the Hf4 "cube" in $Hf_{5.08}Mo_{0.92}P_3$ so that Hf1 in Hf_2P is only coordinated by four phosphorus, and Hf4 in $Hf_{5.08}Mo_{0.92}P_3$ is trigonal bipyramidally coordinated by five phosphorus. Intuitively, M5 and Hf2 in $Hf_{5.08}Mo_{0.92}P_3$ are more metal–metal bonded than the corresponding Hf3 and Hf5 in Hf_2P and Hf4 in $Hf_{5.08}Mo_{0.92}P_3$ is less metal–metal bonded than Hf1 in Hf_2P. Overall, the metal–metal bonding contribution in $Hf_{5.08}Mo_{0.92}P_3$ as discerned from contact alone should be more significant than that in Hf_2P. This observation is consistent with both Pauling bond order calculation and Mulliken overlap population by the extended Hückel method.

Guiner X-ray powder pattern phase analysis was carried out on annealed samples of M_2P with metal stoichiometries ranging from 92 to 9% Hf. A phase width of $(Hf/Mo)_6P_3$ with the new structure type between 92 and 80% Hf is shown by the fact that in all cases this is the major phase. In the composition range of over 80% Hf other types of structures (20) resulted from the melts. An unidentified minor phase was also presented in several powder patterns, and it seems possible that by varying the metal-to-metal ratio and metal-to-phosphorus ratios in the Hf–Mo–P system a new structure might be found (15).

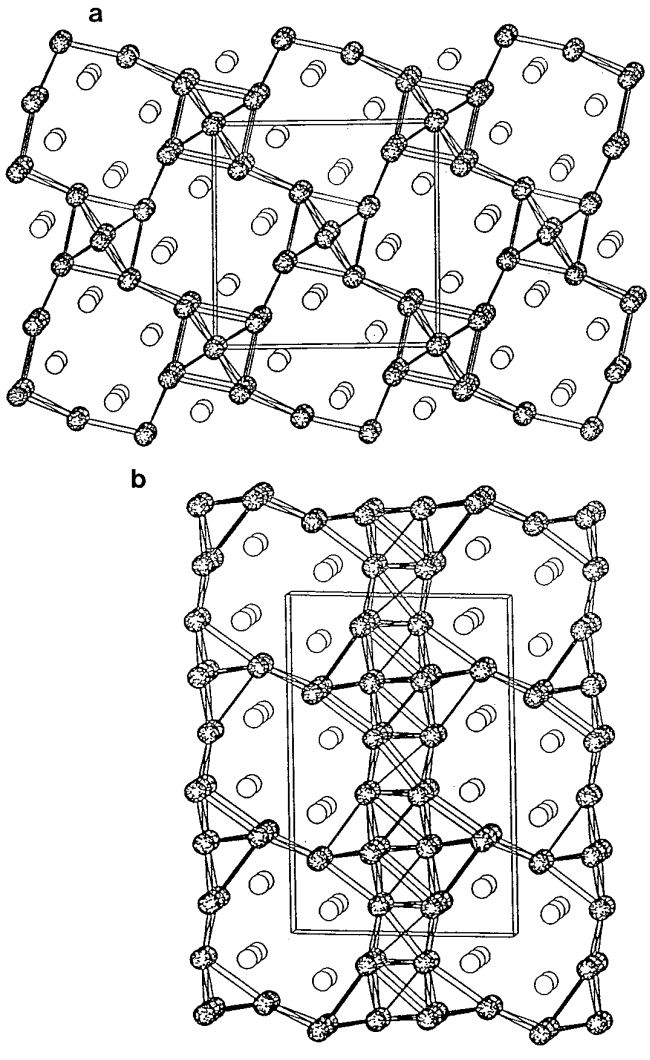

FIG. 6. The structure of Nb_5Se_4 (top) and Nb_2Se (bottom) viewed from the short axes.

BONDING AND BONDING COMPARISONS OF $Hf_{5.08}Mo_{0.92}P_3$ AND Hf_2P

Bond-order calculations (21), making use of the Pauling bond order equation, $D(n) = D(1) - 0.6 \log n$, have been found to be useful not only for locating atoms in a initial structure determination but also in understanding the different site occupancies. The bond order results for the different sites of $Hf_{5.08}Mo_{0.92}P_3$ and Hf_2P are given in Table 5.

Mulliken overlap populations of M–M and M–P for each metal site in Hf_2P and hypothetical M_2P (with the structure of $Hf_{5.08}Mo_{0.92}P_3$) were obtained from band structure calculations using the extended Hückel method (22) (Table 7). Parameters for these calculations are given in Table 6 and parameters of Hf were used for all the metal sites in $Hf_{5.08}Mo_{0.92}P_3$ yielding calculated values for a hypothetical Hf_2P isostructural to the new compound. The correlation of both bond distance with Mulliken overlap population and Pauling bond order with Mulliken overlap population for Hf_2P and $Hf_{5.08}Mo_{0.92}P_3$ are shown in Figs. 8 and 9, respectively. The general trend is that the shorter the bond of the same type (the stronger the bond), the larger the Pauling bond order and the Mulliken overlap population. The correlation of the PBO with MOP is much better than that of the bond distances with MOP. These correlations suggest that both PBO and MOP can be used as scales to evaluate the strength of the metal–metal bonding and metal–phosphorus bonding for each metal site in Hf_2P and $Hf_{5.08}Mo_{0.92}P_3$. In Hf_2P, POB M–M) gives values for each Hf site as Hf6 > Hf3 > Hf1 > Hf5 ≈ Hf4 > Hf2 while MOP (M–M) gives Hf6 ≈ Hf3 > Hf1 > Hf5 > Hf4 ≈ Hf2, POB (M–P) gives Hf2 > Hf4 > Hf5 > Hf1 ≈ Hf6 > Hf3, and MOP (M–P) gives Hf2 > Hf4 > Hf1 ≈ Hf5 > Hf6 ≈ Hf3. These results support the observations that the Hf3 and Hf6 sites (each has three phosphorous neighbors) are the strongest metal–metal bonding and the weakest metal–phosphorus bonding sites, while the Hf2 and Hf4 sites (each has five phosphorous neighbors) are the strongest metal–phosphorus bonding sites. The Hf1 and Hf5 (each has four phosphorous neighbors) are the intermediate in

TABLE 5
Pauling Bond Orders (PBO) for $Hf_{5.08}Mo_{0.92}P_3$ and Hf_2P

$Hf_{5.08}Mo_{0.92}P$				Hf_2P			
Atoms	Total	M–M	M–P	Atoms	Total	M–M	M–P
M1	5.67	1.98	3.69	Hf1	4.85	2.87	1.98
M2	5.27	2.47	2.80	Hf2	5.32	2.14	3.18
M3	5.19	2.13	3.06	Hf3	4.67	3.30	1.37
M4	4.76	2.60	2.16	Hf4	5.24	2.25	2.98
M5	6.16	5.18	0.98	Hf5	4.77	2.26	2.51
M6	5.98	4.11	1.87	Hf6	5.60	3.65	1.95
P1	4.54			P1	5.00		
P2	5.21			P2	4.58		
P3	4.90			P3	4.45		

TABLE 6
Atomic Parameters Used in the Extended Hückel Calculations

Atom	Orbital	H_{ii} (eV)	ζ_1	C_1	ζ_1	C_2
P	3*s*	−18.60	1.68			
	3*p*	−12.50	1.63			
Hf	6*s*	−8.12	2.21			
	6*p*	−4.50	2.17			
	5*d*	−8.14	4.36	0.7145	1.709	0.5458

Note. Double zeta functions are used for Hf.

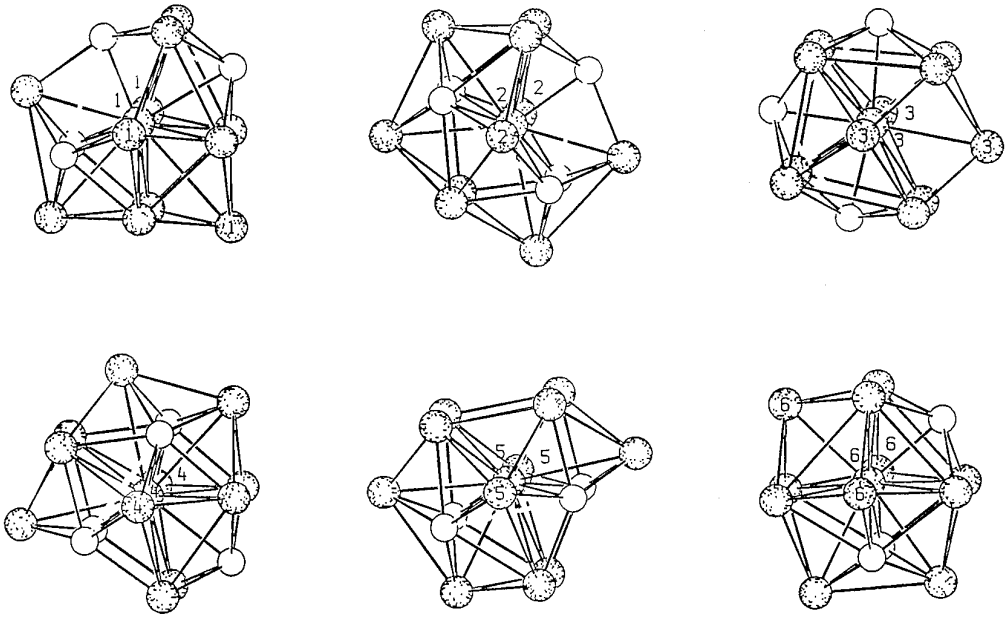

FIG. 7. Six kinds of Hf environments in Hf_2P, Hf1 to Hf3 (top, from right to left) and Hf4 to Hf6 (bottom, from left to right).

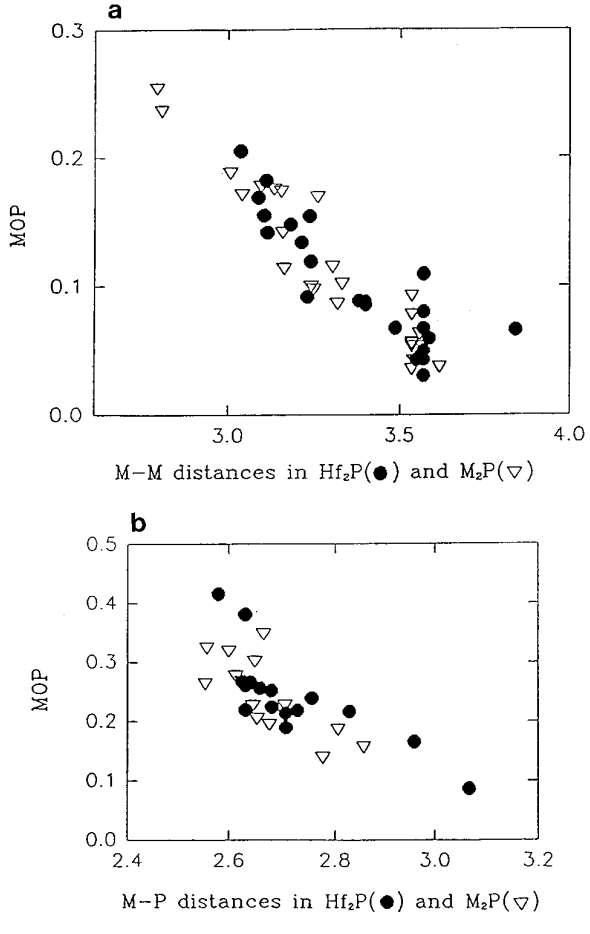

both metal–metal bonding and metal–phosphorous bonding. The total MOPs for the different metal sites from Hf1 to Hf6 are 2.27, 2.38, 2.21, 2.07, 2.04, and 2.32 respectively. In $Hf_{5.08}Mo_{0.92}P_3$, both PBO (M–M) and MOP (M–M) give values for each site as M5 > M6 ⩾ M4 ≈ M2 > M3 > M1, while POB (M–P) gives M1 > M3 > M2 > M4 > M6 > M5 and MOP (M–P) gives M1 > M3 > M4 > M2 > M6 ⩾ M5. M5 and M6 have the largest PBO (M–M) and MOP (M–M), M5 had the smallest PBO (M5–P) and MOP (M5–P), and M6 has the second smallest PBO (M6–P) and MOP (M–P). These results support the structurally motivated suggestion that M5 and M6 are the strongest metal–metal bonding sites, M5 is the weakest metal–phosphorus bonding site and M6 is the second weakest metal–phosphorus bonding site. The total MOP for the different metal sites from M1 to M6 are 2.32, 2.22, 2.12, 2.38, 2.46, and 2.62. Furthermore, in both cases, it is found that (1) the metal–metal bonding increases and the metal–phosphorus bonding decreases with decreased phosphorus coordination numbers, (2) for metals with the same number of phosphorus neighbors, the differences of metal–metal bonding or metal–phosphorus bonding among those metals are small, and (3) Mulliken overlap populations generally give better correlations than PBO.

The previous intuitive metal–site comparison between

FIG. 8. The correlations of MOP with metal–metal distances (top) and MOP with metal–phosphorus distances (bottom) in Hf_2P and M_2P ($Hf_{5.08}Mo_{0.92}P_3$ structure).

TABLE 7
Mulliken Overlap Populations (MOP) for $Hf_{5.08}Mo_{0.92}P_3$ and Hf_2P[a]

$Hf_{5.08}Mo_{0.92}P_3$						Hf_2P					
M	Tot	*M–M*	*M–M*/*n*	*M–P*	*M–P*/*n*	*M*	Tot	*M–M*	*M–M*/*n*	*M–P*	*M–P*/*n*
Hf1	2.32	1.01	0.10	1.31	0.26	Hf1	2.27	1.33	0.12	0.94	0.24
Hf2	2.22	1.27	0.11	0.95	0.24	Hf2	2.38	0.98	0.10	1.40	0.28
Hf3	2.12	0.99	0.09	1.13	0.23	Hf3	2.21	1.53	0.14	0.68	0.23
Hf4	2.38	1.29	0.13	1.09	0.22	Hf4	2.07	0.93	0.09	1.14	0.23
M5	2.46	2.00	0.17	0.46	0.23	Hf5	2.04	1.13	0.10	0.91	0.23
M6	2.62	1.79	0.16	0.83	0.27	Hf6	2.32	1.59	0.14	0.73	0.24

[a] Tot stands for total MOP. *M* stands for metal site. *M–M*/*n* and *M–P*/*n* stand for MOP per metal–metal bond and per metal–phosphorus bond.

Hf_2P and $Hf_{5.08}Mo_{0.92}P_3$ had shown that Hf1, Hf2, and M6 in $Hf_{5.08}Mo_{0.92}P_3$ have the same environments as Hf2, Hf5, and Hf6 in Hf_2P, respectively, and Hf2, Hf4, and M5 in $Hf_{5.08}Mo_{0.92}P_3$ have similar environment as Hf5, Hf1, and Hf3 in Hf_2P, respectively. The average MOP per M–M bond for each metal site in Hf_2P from Hf1 to Hf6 are 0.12, 0.10, 0.14, 0.09, 0.10, and 0.14, and for $Hf_{5.08}Mo_{0.92}P_3$ from Hf1 to M6 they are 0.10, 0.11, 0.09, 0.13, 0.17, and 0.16. The average MOPs per M–P bond for each metal site in $Hf_{5.08}Mo_{0.92}P_3$ from Hf1 to M6 are 0.26, 0.24, 0.23, 0.22, 0.23, and 0.27, and in Hf_2P from Hf1 to Hf6 they are 0.24, 0.28, 0.23, 0.23, 0.23, and 0.24. Comparing average MOP per bond for the corresponding sites between the two structures, e.g., M5 vs Hf3, M6 vs Hf6, or Hf4 vs Hf1 (the latter always from Hf_2P), the same conclusion can be drawn as the previous intuitive observation. it is also interesting to note that the total number of M–P bonds (20 in total) as well as the average MOP per M–P (MOP_{av} = 0.24) and total MOP for M–P (Δ = MOP_{mp} ($Hf_{5.08}Mo_{0.92}P_3$) − MOP_{mp} (Hf_2P) = −0.02) for both structures are the same, but there are significantly larger total MOP for M–M (Δ = MOP_{mm} ($Hf_{5.08}Mo_{0.92}P_3$) − MOP_{mm} (Hf_2P) = 0.66) for $Hf_{5.08}Mo_{0.92}P_3$ than that for Hf_2P. This supports the idea that the stronger metal–metal bonding character brought

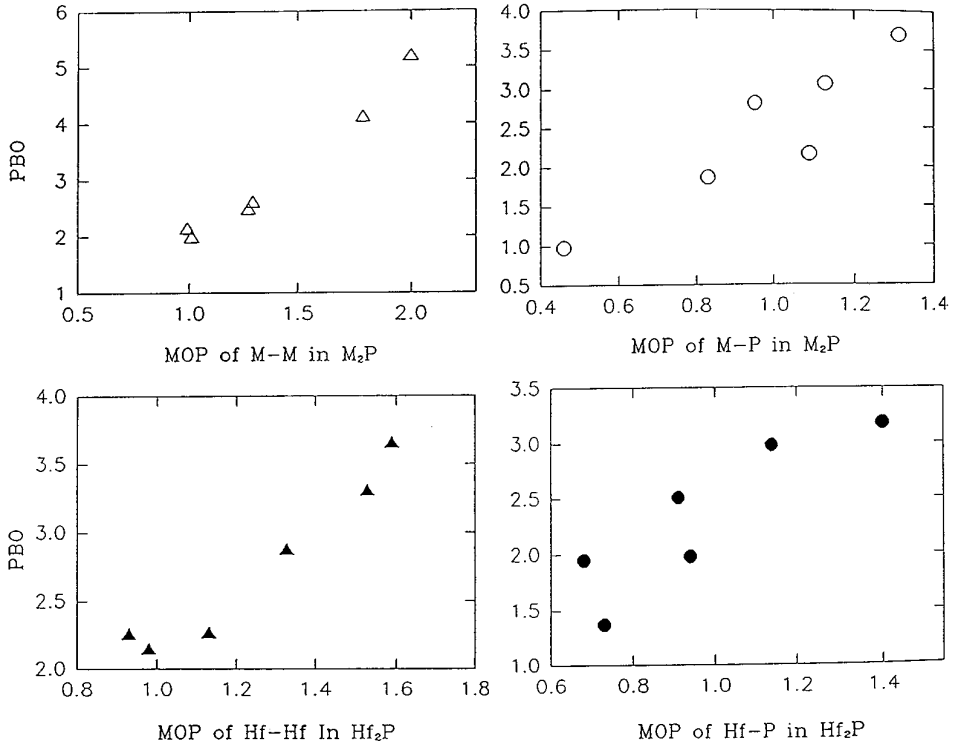

FIG. 9. The correlations of PBO (M–M) with MOP (M–M) (top left) and PBO (M–P) with MOP (M–M) (top right) in M_2P ($Hf_{5.08}Mo_{0.92}P_3$ structure). The correlations of PBO (Hf–Hf) with MOP (Hf–Hf) (bottom left) and PBO (Hf–P) and MOP (Hf–P) (bottom right) in Hf_2P.

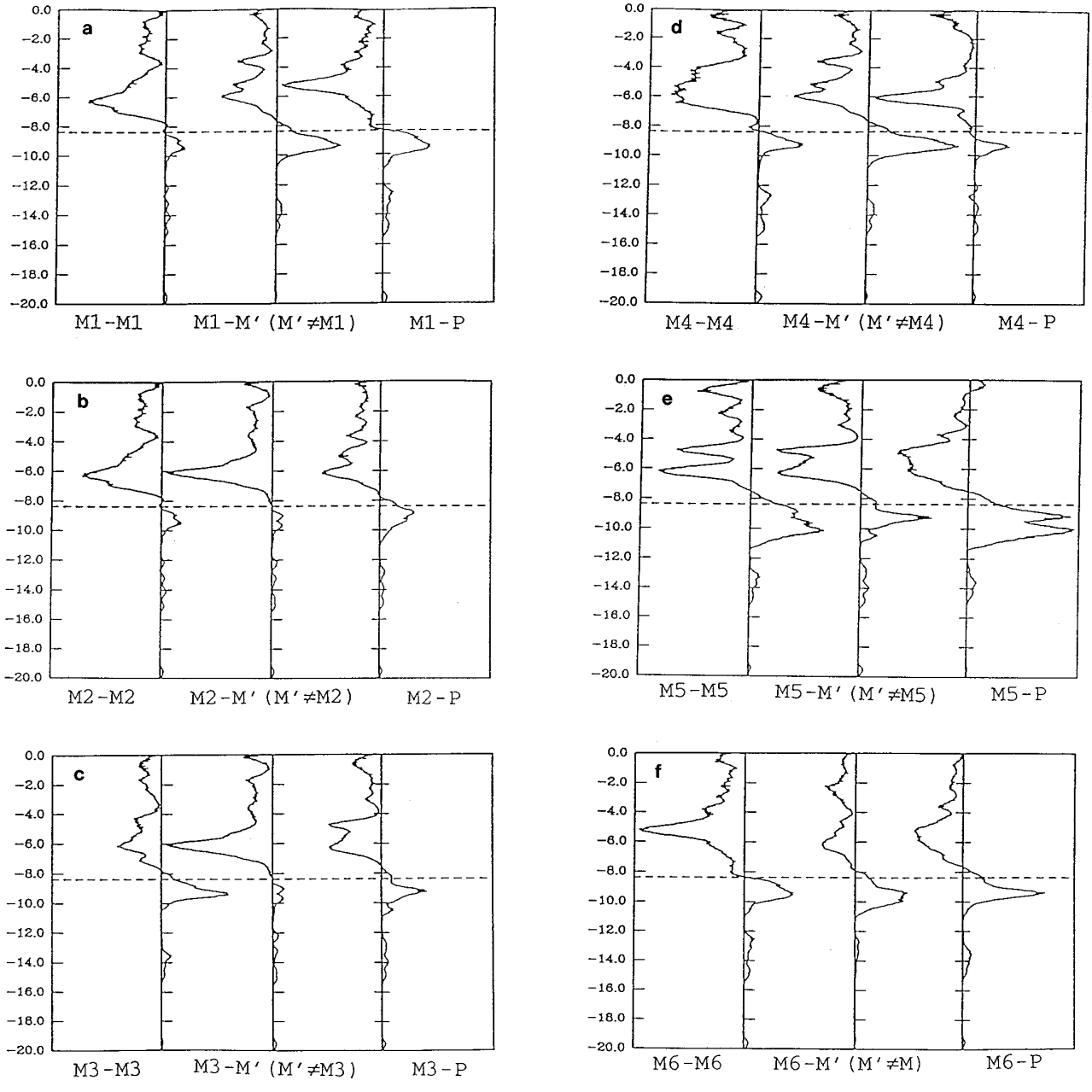

FIG. 10. (a–f) COOP curves for six metal sites in $Hf_{5.08}Mo_{0.92}P_3$.

about by Mo indeed increases the metal–metal bonding contribution in $Hf_{5.08}Mo_{0.92}P_3$, which contributes to the formation of this new structure. On the other hand, the new structure is certainly entropically stabilized by the differential occupancies of the M5 and M6 sites relative to the stoichiometric mixture of Hf_2P and pseudo-binary Mo_2P.

Final problems that need to be addressed are: Why Mo does occupy only the M5 and M6 sites, not the other sites? And why does the M6 site have more Mo than the M5 site? The rule of topological charge stabilization (23), which assess the structure of ternary derivatives by hypothesizing that the more electronegative atoms will occupy the site with the larger Mulliken population, has been used to interpret site preferences in the $(Nb, Ta)_4S_2$ (24) layer structure and ZrNbP(Co_2Si-type) and $Hf_{1.06}Mo_{0.94}P$ (Fe_2P-type) structures. Here this rule is also consistent with the observed occupancies in $Hf_{5.08}Mo_{0.92}P_3$. On any electronegativity scale, $\chi(Mo) > \chi(Hf)$, e.g., the Matynov–Batsanov scale, electronegativity for Hf is 1.73 and for Mo

is 1.94. As for $Hf_{5.08}Mo_{0.92}P_3$, the total MOPs for the sites from M1 to M6 are in the decreasing order M6 > M5 > Hf4 > Hf1 > Hf2 > Hf3 with values of 2.62, 2.46, 2.38, 2.32, 2.22, and 2.12, respectively. Obviously, the M6 site has the largest and the M5 site has the second largest total MOP. So Mo should prefer to occupy the M6 and M5. But here the differences among the total MOP of the M6 and M5 sites and the other sites range from 0.08 to 0.50 in $Hf_{5.08}Mo_{0.92}P_3$, compared with MOP differences in ZrNbP and $Hf_{1.06}Mo_{0.94}P$, which are 0.54 and 0.81. Recently, ''COOP optimization'' (25–26) for metal–metal bonding has been observed in several metal-rich compounds. By examining the COOP curve of for each metal site of $Hf_{5.08}Mo_{0.92}P_3$ (Figs. 10a–10f), ''COOP optimization'' (i.e., optimization of metal–metal bonding or metal–phosphorus bonding) of some bonds, discussed below, appears to be provided. The COOPs are optimized by Hf1–Hf1 and Hf1–P bonding for the Hf1 site, Hf2–Hf2 and Hf2–M' ($M' \neq$ Hf2) bonding for the Hf2 site, Hf3–M' ($M' \neq$ Hf3) bonding for the Hf3 site, Hf4–Hf4 and Hf4–P bonding for the Hf4 site, and M6–M6 bonding for M6 sites, while for the M5 site none of the bonds have been optimized and there remain states that could accommodate additional electrons. This suggests that all the metal sites except M5 have almost-optimized (or saturated) occupancy, and that further substitution of Hf for Mo in $Hf_{5.08}Mo_{0.92}P_3$ will occur preferentially in the M5 site.

ACKNOWLEDGMENTS

The authors thank Dr. L. Hoistad and Dr. G. Miller for valuable discussion. The Ames Laboratory is operated for the Department of Energy by Iowa State University under Contract W-7405-Eng-82. This research was supported by the U.S. Department of Energy, Office of Basic Energy Sciences, materials Sciences Division.

REFERENCES

1. H. F. Franzen, *Prog. Solid State Chem.* **12,** 1 (1978).
2. J. P. Owens, B. R. Conard, and H. F. Franzen, *Acta Crystallogr.* **23,** 77 (1967).
3. J. P. Owens and H. F. Franzen, *Acta Crystallogr.* **30B,** 427 (1974).
4. S. Rundqvist, *Acta Chem. Scand.* **20,** 2427 (1966).
5. L. E. Tergenius, B. I. Nolang, and T. Lundstrom, *Acta Chem. Scand. Ser. A Phys. Inorg. Chem.* **35A,** 693 (1981).
6. H. F. Franzen, T. A. Beineke, and B. R. Conard, *Acta Crystallogr.* **B24,** 412 (1968).
7. H. Y. Chen, R. T. Tuenge, and H. F. Franzen, *Inorg. Chem.* **12,** 552 (1973).
8. X. Yao and H. F. Franzen, *J. Solid State Chem.* **86,** 88 (1990).
9. X. Yao and H. F. Franzen, *Z. Anorg. Allg. Chem.* **598/599,** 353 (1991).
10. G. A. Marking and H. F. Franzen, *Chem. Mater.* **5,** 678 (1993).
11. X. Yao, G. A. Marking, and H. F. Franzen, *Ber. Bursenges. Phys. Chem.* **96,** 1552 (1992).
12. S. Rundqvist, *Acta Chem. Scand.* **19,** 393 (1965).
13. T. Johnsson, *Acta Chem. Scand.* **26,** 365 (1972).
14. B. Sellberg and S. Rundqvist, *Acta Chem. Scand.* **19,** 760 (1965).
15. J. Cheng and H. F. Franzen, unpublished results.
16. ''CHES: An Empirical Absorption Correction Program Written by Jacobson's Group.''
17. ''Texsan: Single Crystal Analysis Software,'' Version 5.0. Molecular Structure Corporation, The Woodland, TX, 1989.
18. K. Selte and A. Kjekshus, *Acta Chem. Scand.* **17,** 2560 (1963).
19. B. R. Conard, L. J. Norrby, and H. F. Franzen, *Acta Crystallogr. Sect. B* **25B,** 1729 (1969).
20. G. J. Miller and J. Cheng, *Inorg. Chem.*, **34,** 2962 (1995).
21. L. Pauling, ''The Nature of Chemical Bonds'' 3rd ed. Cornell Univ. Press, Ithaca, NY, 1948.
22. (a) M. H. Whangbo and R. Hoffmann, *J. Am. Chem. Soc.* **100,** 6093 (1978); (b) R. Hoffmann, *J. Chem. Phys.* **39,** 1397 (1963).
23. (a) B. M. Gimarc, *J. Am. Chem. Soc.* **105,** 1979 (1983); (b) J. K. Burdett, *Prog. Solid State Chem.* **15,** 173 (1984).
24. X. Yao, G. J. Miller, and H. F. Franzen, *J. Alloys Comp.* **183,** 7 (1992).
25. K. S. Nanjundaswamy and T. Hughbank, *J. Solid State Chem.* **98,** 278 (1992).
26. T. Hughbank, *Prog. Solid State Chem.* **19,** 329 (1989).